Shape memory alloy helical springs: modeling, simulation and experimental analysis

Ricardo Alexandre Amar de Aguiar
CEFET/RJ - Department of Mechanical Engineering, Rio de Janeiro/RJ – Brazil

Juliana Hoyer Insaurrauld Pereira, Cristina Gomes de Souza
CEFET/RJ - PPTEC / Department of Mechanical Engineering, Rio de Janeiro/RJ – Brazil

Pedro Manuel Calas Lopes Pacheco
CEFET/RJ - PPEMM / Department of Mechanical Engineering, Rio de Janeiro/RJ – Brazil

Marcelo Amorim Savi
COPPE/UFRJ - Department of Mechanical Engineering, Rio de Janeiro/RJ – Brazil

Abstract

Shape memory alloys (SMAs) are metallic materials that have the capability to recover its original shape eliminating residual deformations when subjected to adequate thermal process. This behavior is related to phase transformation induced by stress or temperature and several alloys present this behavior. During the phase transformation process of a SMA component, large loads and/or displacements can be generated in a relatively short period of time making this component an interesting mechanical actuator. Because of such remarkable properties, SMAs have found a number of applications in different areas. The present contribution deals with the modeling, simulation and experimental analysis of SMA helical springs. Basically, it is assumed a one-dimensional constitutive model to describe its thermomechanical shear behavior and, afterwards, helical springs are modeled by considering classical approach. A numerical method based on the operator split technique is developed. SMA helical spring thermomechanical behavior is investigated through experimental tests performed at different loads. Numerical results show that the model is in close agreement with those obtained by experimental tests.

Keywords: shape memory alloy, modeling, helical spring, experimental analysis.

Mechanics of Solids in Brazil 2009, H.S. da Costa Mattos & Marcílio Alves (Editors)
Brazilian Society of Mechanical Sciences and Engineering, ISBN 978-85-85769-43-7

1 Introduction

Shape memory alloys (SMAs) present complex thermomechanical behaviors related to different physical processes. The most common phenomena presented by this class of material are the pseudoelasticity, the shape memory effect, which may be one-way (SME) or two-way (TWSME), and the phase transformation due to temperature variation. Besides these phenomena, there are more complicated effects that have significant influence over its overall thermomechanical behavior – for instance: plastic behavior, tension-compression asymmetry, plastic-phase transformation coupling, transformation induced plasticity, thermomechanical coupling, among others [1, 2]. The remarkable properties of SMAs are attracting much technological interest, motivating different applications in several fields of sciences and engineering. Aerospace, biomedical, and robotics are some areas where SMAs have been applied [3–15].

SMAs have the capability to generate large strains associated with phase transformation induced by stress and/or temperature variations [3, 16]. During the phase transformation process of a SMA component, large loads and/or displacements can be generated in a relatively short period of time making this component an interesting mechanical actuator. Basically, SMA presents two possible phases: martensite and austenite. Martensitic phase may appear in variants induced by different kinds of stress fields [17]. Several alloys can develop strains associated with phase transformation but only those that can develop large strains are of commercial interest, as nickel-titanium (NiTi) and copper base alloys (CuZnAl and CuAlNi).

SME occurs at low temperatures, below a critical temperature where twined martensite phase is the only stable phase in a stress-free state (M_F). Figure 1a presents a stress-strain curve for the shape memory effect at a constant temperature. For this situation the nonlinear behavior in the loading process is associated with phase transformation related to the conversion from twinned to detwinned martensite ($O \rightarrow A \rightarrow B$). After the unloading process (C), some amount of residual strain remains (ϵ_R), meaning that the reverse transformation is not completed. The shape memory effect takes place by heating the alloy at a temperature above a critical temperature (A_F) where austenitic phase is the only stable phase in a stress-free state. This temperature change controls the transformation from detwinned martensite to austenite and promotes the residual strain recovery. Figure 1b presents a diagram that illustrates the shape memory effect. M_S and M_F are the temperatures at which the formation of martensite starts and ends, respectively, while A_S and A_F are the temperatures at which the formation of austenite starts and ends, respectively.

The complex thermomechanical behavior of SMAs makes their modeling a difficult task. This may introduce difficulties in the evaluation of SMA applications. SMA springs are an important actuator that can be used in different kinds of application. There are some efforts to model the SMA helical springs thermomechanical behavior [18–20]. In the present contribution, it is proposed a model that may be useful for engineering purposes. Basically, a constitutive model originally proposed for one-dimensional tensile-compressive behavior [2, 21–23] is employed to describe the shear behavior. Afterwards, it is developed a SMA helical spring model by assuming that the spring wire presents a homogeneous phase transformation. An experimental apparatus is developed in order to characterize the thermomechanical behavior of SMA helical springs through load-displacement tests. Finally,

Mechanics of Solids in Brazil 2009, H.S. da Costa Mattos & Marcílio Alves (Editors)
Brazilian Society of Mechanical Sciences and Engineering, ISBN 978-85-85769-43-7

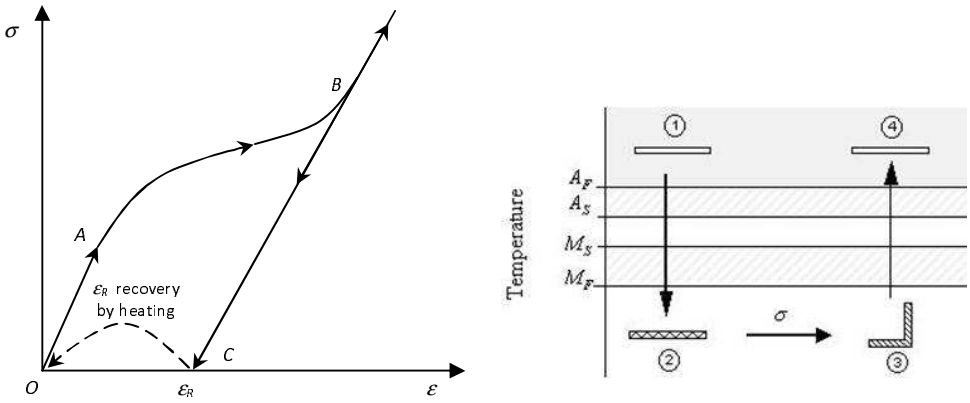

(a) (b)

Figure 1: Shape memory effect (SME). Stress-strain curve (a) and a diagram to illustrate the shape memory effect (b).

numerical simulations are carried out showing that the proposed model is in close agreement with experimental tests.

2 Constitutive model

There are different ways to describe the thermomechanical behavior of SMAs [24]. Here, a constitutive model that is built upon the Fremond's model [25, 26] and previously presented in different references [2, 21–23] is employed. This model considers different material properties and four macroscopic phases for the description of the SMA behavior. The model also considers plastic strains and plastic-phase transformation coupling, which turns possible the two-way shape memory effect description. Moreover, the original model also contemplates tension-compression asymmetry.

Besides strain (ϵ) and temperature (T), the model considers four more state variables associated with the volumetric fraction of each phase: β_1 is associated with tensile detwinned martensite, β_2 is related to compressive detwinned martensite, β_3 represents austenite and β_4 corresponds to twinned martensite. Actually, the original model also includes other variables related to plastic phenomenon, which are beyond the scope of this contribution.

Although this one-dimensional constitutive model is originally proposed to describe tension-compression behavior, it has been noted that experimental torsion test curves presented in different references [27, 28] indicate that these curves are qualitatively similar to those obtained in tension tests performed in Ni-Ti and other SMAs. Based on this observation, this constitutive model is employed to describe the pure shear stress states, replacing the stress, strain, and elastic modulus respectively by the shear stress τ, shear strain γ, and shear modulus G.

In order to obtain the constitutive equations a free energy potential is proposed concerning each isolated phase. After this definition, a free energy of the mixture can be written weighting each energy function with its volumetric fraction. With this assumption, it is possible to obtain a complete set of constitutive equations that describes the thermomechanical behavior of SMAs as presented bellow:

$$\tau = G\gamma + (\alpha + G\alpha_h)(\beta_2 - \beta_1) \tag{1}$$

$$\dot{\beta}_1 = \frac{1}{\eta_1}\left\{ \alpha\gamma + \Lambda_1 + \left(2\,\alpha_h\alpha + G\,\alpha^2\right)(\beta_2 - \beta_1) + \alpha_h G\,\gamma - \partial_1 J_\pi \right\} + \partial_1 J_\chi \tag{2}$$

$$\dot{\beta}_2 = \frac{1}{\eta_2}\left\{ -\alpha\gamma + \Lambda_2 - \left(2\,\alpha_h\alpha + G\,\alpha^2\right)(\beta_2 - \beta_1) - \alpha_h G\,\gamma - \partial_2 J_\pi \right\} + \partial_2 J_\chi \tag{3}$$

$$\dot{\beta}_3 = \frac{1}{\eta_3}\left\{ -\frac{1}{2}\,(G_A - G_M)\,[\gamma + \alpha_h(\beta_2 - \beta_1)]^2 + \Lambda_3 - \partial_3 J_\pi \right\} + \partial_3 J_\chi \tag{4}$$

where $G = G_M + \beta_3\,(G_A - G_M)$ is the shear modulus. Note that subscript "A" refers to austenitic phase, while "M" refers to martensite. Parameters α and α_h are respectively associated with the vertical and horizontal sizes of the stress-strain hysteresis loop. The terms $\partial_n J_\pi$ (n = 1,2,3) are sub-differentials of the indicator function J_π with respect to βn [29]. The indicator function J_π $(\beta_1, \beta_2, \beta_3)$ is related to a convex set π, which provides the internal constraints related to the phases' coexistence. Concerning the evolution equations of volumetric fractions, η_1, η_2 and η_3 represent the internal dissipation related to phase transformations. Moreover, $\partial_n J_\chi$ (n = 1,2,3) are sub-differentials of the indicator function J_χ with respect to $\dot{\beta}_n$ [29]. This indicator function is associated with the convex set χ, which establishes conditions for the correct description of internal sub-loops due to incomplete phase transformations and also avoids phase transformations $M+ \rightarrow M$ or $M- \rightarrow M$ [23].

Concerning the parameters definition, linear temperature dependent relations are adopted for Λ_1, Λ_2 and Λ_3 as follows:

$$\Lambda_1 = \Lambda_2 = -L_0^M + \frac{L^M}{T_M}(T - T_M) \qquad \Lambda_3 = -L_0^A + \frac{L^A}{T_M}(T - T_M) \tag{5}$$

where T_M is the temperature below which the martensitic phase becomes stable, L_0^M, L^M, L_0^A and L^A are parameters related to critical stress for phase transformation.

In order to contemplate different characteristics of the kinetics of phase transformation for loading and unloading processes, it is possible to consider different values to the parameters η_n (n = 1,2,3), which are related to internal dissipation: η_n^L and η_n^U during loading and unloading process, respectively. For more details about the constitutive model, see Paiva *et al.* [22].

3 Shape memory alloy helical spring

The modeling of the restoring force produced by a shape memory alloy spring is done considering a helical spring with diameter D, built with N coils with a wire diameter d. It is assumed that the

longitudinal force, F, is resisted by the torsional shear stress developed on the circular cross section of the helical shaped wire (Fig. 2) [30].

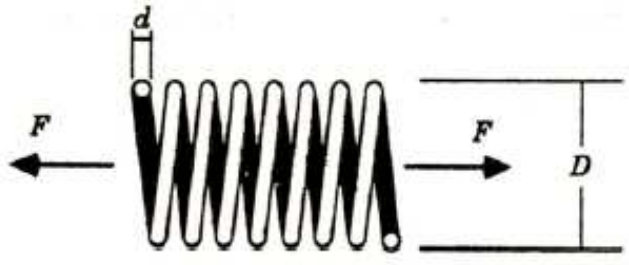

Figure 2: Helical spring.

$$F = \frac{4\pi}{D}\int_0^{d/2} \tau\, r^2 dr \tag{6}$$

where r is the radial coordinate along the wire cross section. It is also assumed that the shear strain is linearly distributed along the wire cross section, from what follows the kinematics relation

$$\gamma = \frac{d}{\pi D^2 N} u \tag{7}$$

where u is the spring displacement.

By combining these equations, and performing the integration, assuming that the wire presents a homogeneous phase transformation through the wire cross section, we obtain:

$$F(u, T, \beta_i) = \frac{\pi\, d^3}{6D}\left[\left(\frac{d}{\pi\, D^2 N} G\right) u + (\alpha + G\alpha_h)\,(\beta_2 - \beta_1)\right] \tag{8}$$

This equation together with those that describes the volume fraction evolution establishes a proper description of the thermomechanical behavior of SMA helical springs.

4 Experimental procedure

The characterization of the SMA helical springs is obtained through load-displacement tests using the tensile test device shown in Fig. 3. This device is composed by a rigid frame that has a load cell (Alfa SV-20 with 20 N capacity) fixed at the top. An SMA spring is connected to the load cell and the other end is attached to the rod of a resistive displacement transducer (Gefran PY-1-F-100 with 100 mm span). Both transducers are connected to a data acquisition system (HBM Spider 8). A

fluid reservoir is attached to the other end of the transducer rod in order to produce the mechanical loadings. The load is prescribed to the SMA spring by controlling the fluid level of the reservoir which is done by changing the vertical position of a second fluid reservoir that is connected to the first by a tube. This configuration allows one to apply precise loading and unloading conditions to the spring element. Temperature variations are induced in the SMA helical spring through joule effect by the application of an electrical current using a stabilized current source (Minipa MPL-1303). The thermomechanical tests developed are composed by two stages: (1) a mechanical loading-unloading followed by a (2) thermal heating-cooling. The first stage promotes a residual strain that is eliminated during the second stage. Three different levels of loads are considered: 3 N, 3.5 N and 4 N. The heating SMA helical spring to a temperature above A_F is performed by applying an electrical current of 1.2 A. All tests are performed at room temperature (22°C).

The SMA helical is built with NiTi that is in martensitic phase at room temperature. The spring has an external diameter of 6 mm, a wire diameter of 0.75 mm, 20 active coils and an activation temperature in the range of 45-55°C.

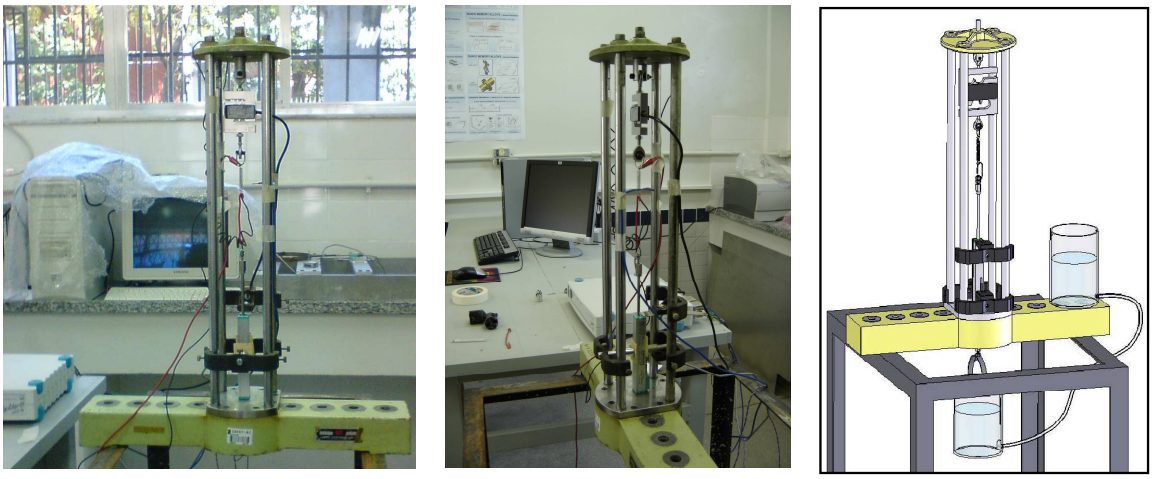

Figure 3: Tensile test device for thermomechanical characterization of the SMA helical springs.

Figure 4 shows the spring load-displacement curves for three different load levels revealing the SME. At the beginning of the test, the SMA helical spring is at room temperature (22°C), a situation where martensitic phase is stable. In order to assure that each test is done with a spring where its wire section has a homogeneous twinned martensitic phase distribution, the following process is applied. Initially, all mechanical loads are removed and then, an electric current of 1.2 A is applied to the spring. Finally, the spring is subjected to cooling prescribed in order to allow a thermal equilibrium with the medium. After this initial treatment, a mechanical loading is applied promoting the formation of detwined martensite that remains after the mechanical load removal causing a residual displacement. At this

point, an electric current of 1.2 A is applied and the SMA helical spring recovers part of the residual displacement developed during the loading stage. A residual load with a magnitude of approximately 1 N is still present at the end of the unloading as a consequence of the devices attached to the spring (resistive displacement transducer, fluid reservoir, etc). A loading rate of approximately 2.7 x 10^{-2} N/s is used in the developed tests.

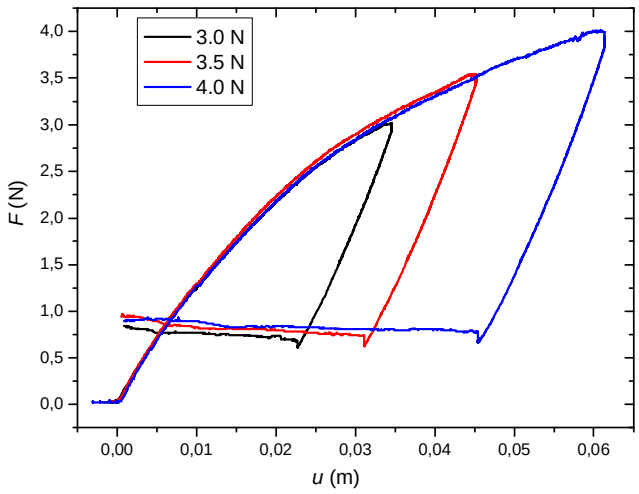

Figure 4: Experimental data related to the spring load-displacement curve for three load levels.

Experimental data is used to match parameters of the proposed model. In the beginning of the test, phase transformation does not take place and the initial slope of the load-displacement curve can be used to obtain $G = 8.5$ GPa. The residual displacement is also employed to match parameters related to phase transformations.

5 Numerical simulations

The operator split technique [31] associated with an iterative numerical procedure is developed in order to deal with the nonlinearities of the formulation. The procedure isolates the sub-differentials and uses the implicit Euler method combined with an orthogonal projection algorithm [2] to evaluate evolution equations. Orthogonal projections assure that volume fractions of the macroscopic phases obey the imposed constraints. In order to satisfy constraints, values of volume fractions must stay inside or on the boundary the tetrahedron shown in Fig. 5 that establishes the phase coexistence conditions.

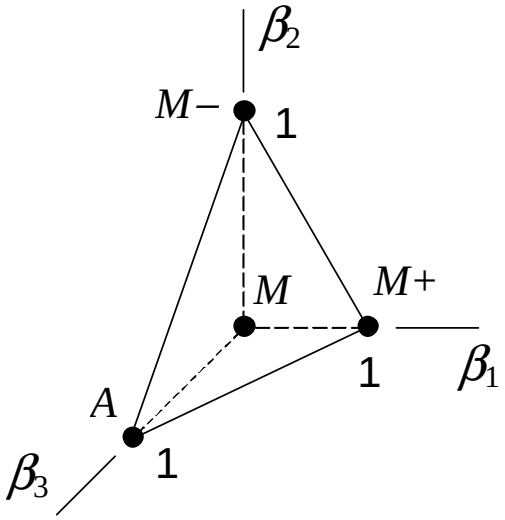

Figure 5: Tetrahedron of the constraints related to phase coexistence.

Numerical simulations are now focused on establishing a comparison with experimental tests. It is considered a helical spring with the same characteristics described in the previous section. Parameters experimentally matched from experimental tests are presented in Table 1.

Table 1: SMA parameters.

G_A(GPa)	G_M(GPa)	α(MPa)	γ_R	T_M (K)
16	8.5	30	0.030	318
L_0^M(MPa)	L^M(MPa)	L_0^A(MPa)	L^A(MPa)	
0.7	9.5	0.03	27	
$\eta_{1,2}^L$(MPa.s)	$\eta_{1,2}^U$(MPa.s)	η_3^L(kPa.s)	η_3^U(kPa.s)	
200	200	150	150	

Figure 6 shows thermomechanical loading that represents the experimental tests: a mechanical loading-unloading followed by a thermal heating-cooling. Figures 7 and 8 present the force-displacement curves and the volume fraction time evolution, respectively, for the three loading levels applied in the experimental tests (3 N, 3.5 N and 4 N). The force-displacement curves have the same behavior

observed in experimental tests, presenting a residual displacement and a load when the mechanical loading-unloading process is finished. Figure 8 allows a better comprehension of the phase transformation process related to this thermomechanical loading process. Initially, martensitic reorientation takes place due to mechanical loading, changing twinned to detwinned martensite. The final state for each of the three load levels is the following: 0.25 for $F = 3$ N, 0.40 for $F = 3.5$ N and 0.60 for $F = 4$ N. Afterwards, during the heating-cooling process, there is an austenitic formation during the heating stage followed by twinned martensite formation during the cooling stage.

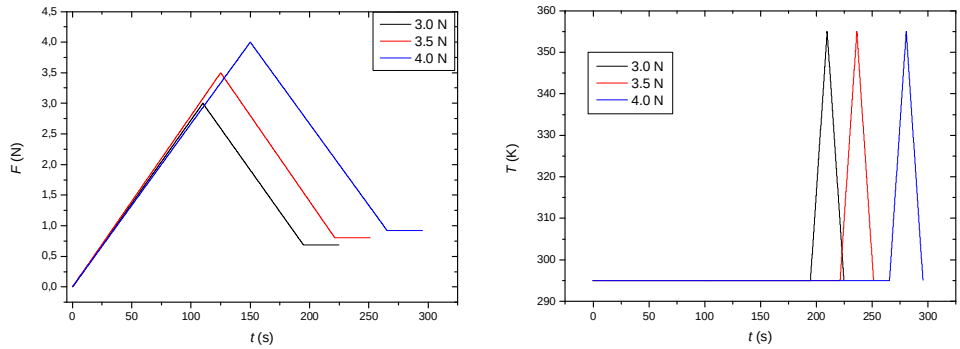

(a) (b)

Figure 6: Thermomechanical loading for three loading levels. (a) Mechanical and (b) thermal loadings.

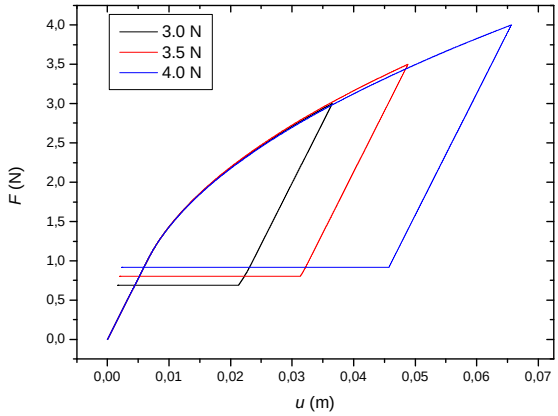

Figure 7: Spring load-displacement curve for three load levels: Numerical simulation.

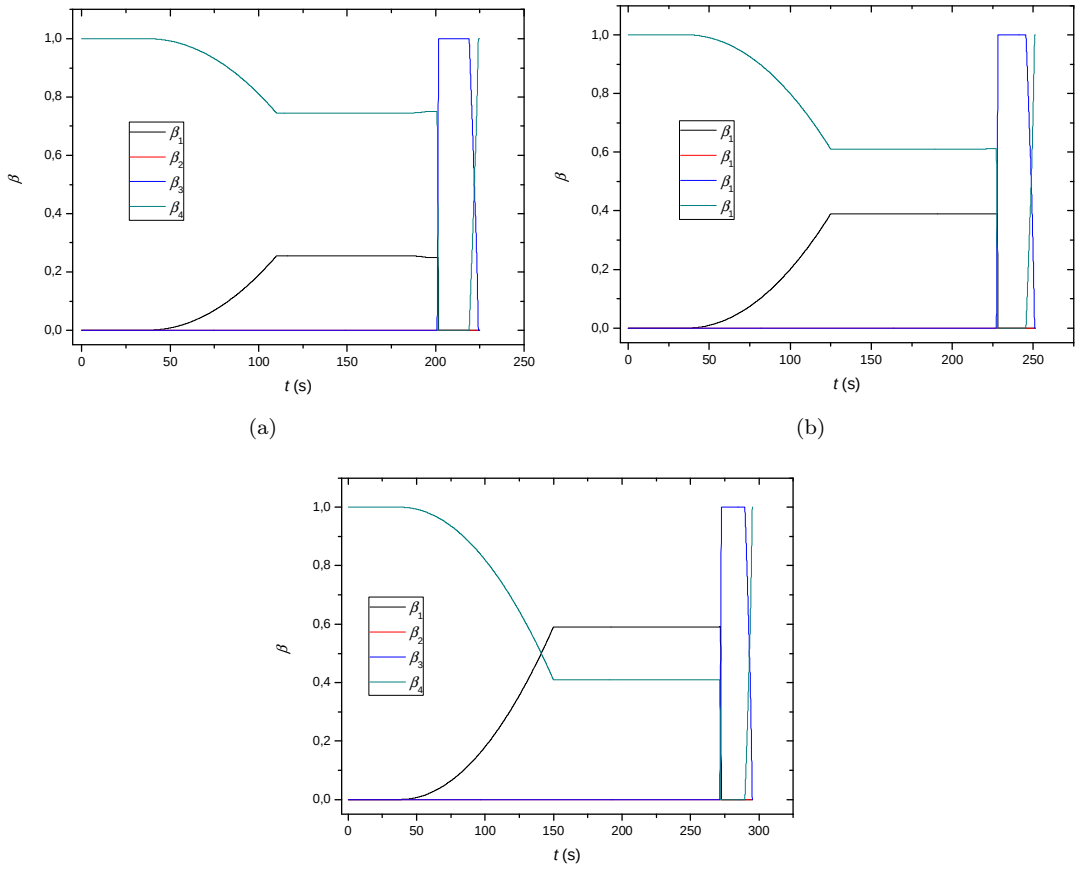

Figure 8: Volume fraction time evolution. (a) $F = 3$ N, (b) $F = 3.5$ N and (c) $F = 4$ N.

In order to establish a comparison between numerical and experimental tests Fig. 9 presents a direct comparison of the load-displacement curves obtained for three load levels analyzed. Results show that model results are in close agreement with experimental tests.

6 Conclusion

This contribution analyses the quasi-static response of shape memory alloy helical springs described by a one-dimensional constitutive model that includes four macroscopic phases in the formulation (three variants of martensite and an austenitic phase) and is used to describe the thermomechanical

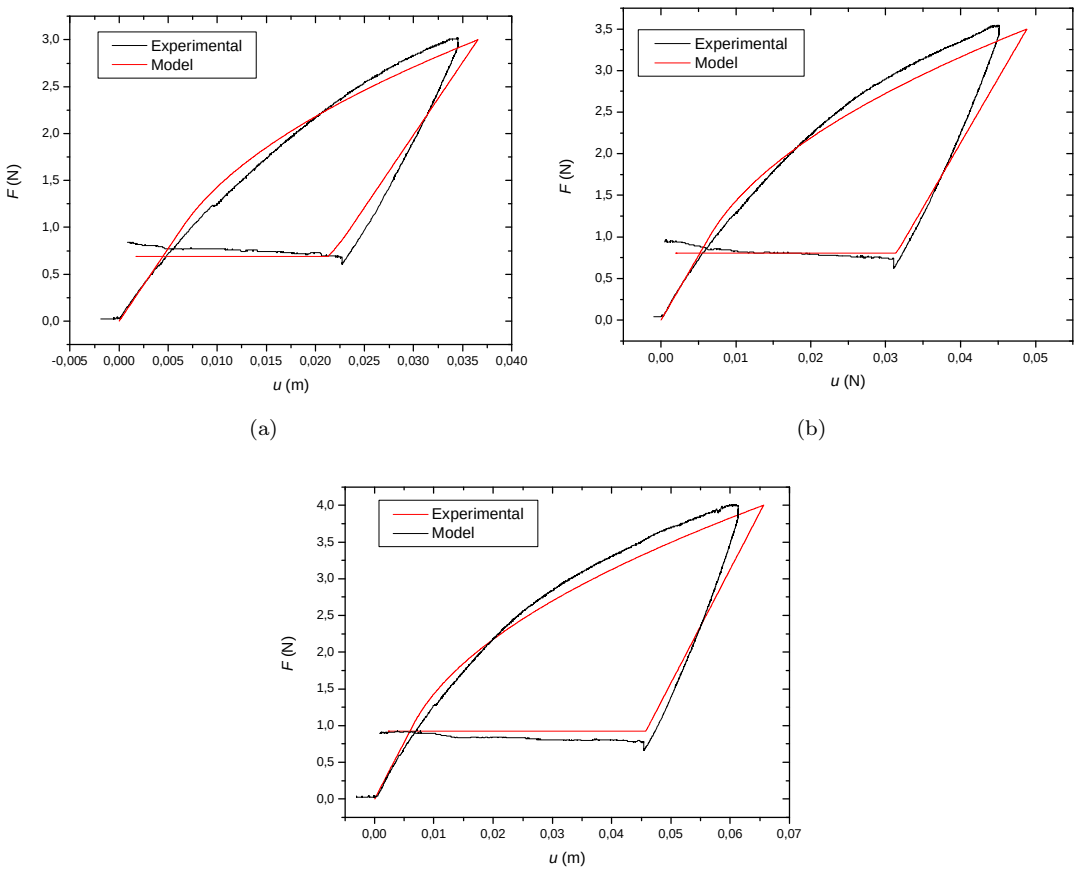

Figure 9: Comparison between experimental and numerical tests of an SMA spring. Load-displacement curve for three load levels. (a) $F = 3$ N, (b) $F = 3.5$ N and (c) $F = 4$ N.

shear behavior of SMA helical springs. A numerical method based on the operator split technique is employed. An experimental apparatus is developed in order to characterize the thermomechanical behavior of SMA helical springs through load-displacement tests. Numerical results show that the proposed model is in close agreement with experimental data obtained and can be used for the design of actuator using SMA helical springs. It is important to highlight that the hypotheses that phase transformation occurs in a homogeneous way at the SMA wire is realistic providing good results.

Acknowledgements

The authors would like to acknowledge the support of the Brazilian Research Agency CNPq and the State Research Agency FAPERJ.

References

[1] Tanaka, K., A phenomenological description on thermomechanical behavior of shape memory alloys. *Journal of Pressure Vessel Technology*, **112**, pp. 158–163, 1990.
[2] Savi, M.A., Paiva, A., Baêta-Neves, A.P. & Pacheco, P.M.C.L., Phenomenological modeling and numerical simulation of shape memory alloys: A thermo-plastic-phase transformation coupled model. *Journal of Intelligent Material Systems and Structures*, **13(5)**, pp. 261–273, 2002.
[3] Rogers, C.A., Intelligent materials. *Scientific American*, pp. 122–127, 1995.
[4] Birman, V., Review of mechanics of shape memory alloys structures. *Applied Mechanics Rev*, **50(11)**, pp. 629–645, 1997.
[5] Pacheco, P.M.C.L. & Savi, M.A., A non-explosive release device for aerospace applications using shape memory alloys. *Proceedings of XIV the Brazilian Congress of Mechanical Engineering (COBEM 97 - ABCM)*, Bauru, Brazil, 1997.
[6] Pacheco, P.M.C.L. & Savi, M.A., Modeling a shape memory release device for aerospace applications. *Revista de Engenharia e Ciências Aplicadas, UNESP*, 2000.
[7] van Humbeeck, J., Non-medical applications of shape memory alloys. *Materials Science and Engineering A*, **273-275**, pp. 134–148, 1999.
[8] La Cava, C.A.P.L., Pacheco, P.M.C.L. & Savi, M.A., Modelagem de um dispositivo de pré-carga com memória de forma para juntas flangeadas. *CONEM 2000 – Congresso Nacional de Engenharia Mecânica*, Natal-RN, 2000.
[9] Webb, G., Wilson, L., D.C., Lagoudas & Rediniotis, O., Adaptive control of shape memory alloy actuators for underwater biomimetic applications. *AIAA Journal*, **38(2)**, pp. 325–334, 2000.
[10] Denoyer, K.K., Scott Erwin, R. & Rory Ninneman, R., Advanced smart structures flight experiments for precision spacecraft. *Acta Astronautica*, **47**, pp. 389–397, 2000.
[11] Garner, L.J., Wilson, L.N., Lagoudas, D.C. & Rediniotis, O.K., Development of a shape memory alloy actuated biomimetic vehicle. *Smart Materials and Structures*, **9(5)**, pp. 673–683, 2001.
[12] Machado, L.G. & Savi, M.A., Odontological applications of shape memory alloys. *Revista Brasileira de Odontologia*, **59(5)**, pp. 302–306, 2002. (in portuguese).
[13] Machado, L.G. & Savi, M.A., Medical applications of shape memory alloys. *Brazilian Journal of Medical and Biological Research*, **36(6)**, pp. 683–691, 2003.
[14] Machado, L.G., Savi, M.A. & Pacheco, P.M.C., Nonlinear dynamics and chaos in coupled shape memory oscillators. *International Journal of Solids and Structures*, **40**, pp. 5139–5156, 2003.
[15] Wang, Z.G., Zu, X.D., Feng, X.D., Zhu, S., Bao, J.W. & Wang, L.M., Characteristics of two-way shape memory TiNi springs driven by electrical current. *Materials and Design*, **25**, pp. 699–703, 2004.
[16] Hodgson, D.E., Wu, M.H. & Biermann, R.J., Shape memory alloys. *ASM Handbook*, **2**, pp. 887–902, 1992.
[17] Zhang, X.D., Rogers, C.A. & Liang, C., Modeling of two-way shape memory effect. *ASME - Smart Structures and Materials*, **24**, pp. 79–90, 1991.
[18] Toi, Y., Lee, J.B. & Taya, M., Finite element análisis of superelastic, large deformation behavior of shape memory alloy helical springs. *Computer and Structures*, **82**, pp. 1685–1693, 2004.

[19] Savi, M.A. & Braga, A.M.B., Chaotic vibrations of an oscillator with shape memory. *Journal of the Brazilian Society of Mechanical Sciences and Engineering*, **XV(1)**, pp. 1–20, 1993.
[20] Tobushi, H. & Tanaka, K., Deformation of a shape memory alloy helical spring - (Analysis based on stress-strain-temperature relation). *JSME International Journal Series I - Solid Mechanics Strength of Materials*, **34(1)**, pp. 83–89, 1991.
[21] Baêta-Neves, A.P., Savi, M.A. & Pacheco, P.M.C.L., On the fremond's constitutive model for shape memory alloys. *Mechanics Research Communications*, **31(6)**, pp. 677–688, 2004.
[22] Paiva, A., Savi, M.A., Braga, A.M.B. & Pacheco, P.M.C.L., A constitutive model for shape memory alloys considering tensile-compressive asymmetry and plasticity. *International Journal of Solids and Structures*, **42(11-12)**, pp. 3439–3457, 2005.
[23] Savi, M.A. & Paiva, A., Describing internal subloops due to incomplete phase transformations in shape memory alloys. *Archive of Applied Mechanics*, **74(9)**, pp. 637–647, 2005.
[24] Paiva, A. & Savi, M.A., An overview of constitutive models for shape memory alloys. *Mathematical Problems in Engineering*, **2006**, pp. 1–30, 2006. Article ID56876.
[25] Fremond, M., Matériaux à mémoire de forme. *C R Acad Sc Paris*, **Tome 34, s.II(7)**, pp. 239–244, 1987.
[26] Fremond, M., *Shape memory alloy: A thermomechanical macroscopic theory*. CISM courses and lectures, Springer Verlag, 1996.
[27] Jackson, C.M., Wagner, H.J. & Wasilewski, R.J., 55-Nitinol - The alloy with a memory: Its physical metallurgy, properties, and applications. *NASA-SP-5110*, 1972.
[28] Manach, P.Y. & Favier, D., Shear and tensile thermomechanical behavior of near equiatomic niti alloy. *Materials Science and Engineering A*, **222**, pp. 45–57, 1997.
[29] Rockafellar, R.T., *Convex analysis*. Princeton Press, 1970.
[30] Shigley, J.E. & Mischke, C.R., *Mechanical Engineering Design*. McGraw-Hill, 6th edition, 2001.
[31] Ortiz, M., Pinsky, P.M. & Taylor, R.L., Operator split methods for the numerical solution of the elasto-plastic dynamic problem. *Computer Methods of Applied Mechanics and Engineering*, **39**, pp. 137–157, 1983.

Mechanics of Solids in Brazil 2009, H.S. da Costa Mattos & Marcílio Alves (Editors)
Brazilian Society of Mechanical Sciences and Engineering, ISBN 978-85-85769-43-7